Modeling and Applications of Everting Vine Robots

Joel Hwee

A thesis
submitted in partial fulfillment of
the requirements for the degree of

Master of Science in Mechanical Engineering

University of Washington

2021

Reading Committee:
Blake Hannaford, Chair
Eric Seibel
Xu Chen

Program Authorized to Offer Degree:
Mechanical Engineering

University of Washington

Abstract

Modeling and Applications of Everting Vine Robots

Joel Hwee

Chair of the Supervisory Committee:
Professor Blake Hannaford
Electrical and Computer Engineering

Everted tubes are soft growing robots that excel at passively navigating convoluted and cluttered environments. This thesis will provide evaluation of an inflated beam model applied to everted tubes, and secondly it will outline a proposed application of everted tubes: advanced airway management. Everted tubes have often been modeled as inflated beams to determine transverse and axial buckling conditions. In this study, the assumption is validated by comparing the tip deflection of everted and uneverted beams. The curvature of everted beams deflected under load and by environmental interactions is also shown to match the model. An iterative method for estimating an everted tube's static tip pose within an environment will also be presented. Advanced airway management is a challenging procedure essential in many trauma settings. This thesis proposes a dual balloon, everting airway device that autonomously deploys into the patient's airway. The dual balloon design allows it to safely deploy into the esophagus or trachea. Eversion gives the proposed device a passive mechanical intelligence allowing it to enter the patient's airway without heading control. Results will demonstrate the feasibility, safety, and efficacy of such a device by characterizing the following: minimum pressures and forces required to deploy individual components; the effects of airway anatomy on growth; and the ability to provide a seal using elastic balloons.

TABLE OF CONTENTS

LIST OF FIGURES

GLOSSARY

AIRWAY PRESSURE (AWP): Pressure within the patients lungs

BAG-VALVE-MASK (BVM): A manual resuscitation device

COMBITUBE: A manual SGA device capable of being deployed into the trachea or esophagus

COSSERAT ROD THEORY: A method of modeling 1D slender rods

CUFF PRESSURE (CP): Internal pressure of a sealing mechanism

EPIGLOTTIS: Flap of cartilage that folds down over the trachea when eating or drinking

ESOPHAGEAL SPHINCTER: Muscle at the top of the esophagus, used for opening and closing of esophagus

ENDOTRACHEAL INTUBATION (ETI): The gold standard method of advanced airway management. A tube is expertly placed into a patient's throat sealing it off

EVERSION: A method of growth via tip extension, all new material is pulled from within the tip to lengthen the tube

HARD PALATE: Bony front part of the roof of the mouth

I-GEL: A manual SGA device used for advanced airway management

INTUBATING LARYNGEAL MASK AIRWAY (ILMA): A manual device that an endotracheal tube can be inserted through

LDPE: Low-Density-PolyEthylene plastic

LARYNGEAL MASK AIRWAY (LMA): A manual SGA device used for advanced airway management

LONGITUDINAL LOADING: A load applied parallel to the length of the beam

MUCOSAL PERFUSION: Blood circulation through mucosal tissues

OHCA: Out of Hospital Cardiac Arrest

PHARYNGEAL CAPILLARIES: Capilaries within the pharynx

POSTERIOR PHARYNGEAL WALL: Tissue at the back of the throat, located over the cervical spine

SERIES PNEUMATIC ACTUATOR MOTORS (SPAMS): A series of connected pouches whose nominal length is longer than its inflated length. Used to steer everted tubes.

SUPRAGLOTTIC AIRWAY (SGA): A type of manual devices inserted into the pharynx during advanced airway management

SOFT PALATE: Muscular part of roof of the mouth

TPU: Thermoplastic PolyUrethane plastic

TRANSVERSE LOADING: A load applied perpendicular to the length of the beam

YOUNG'S MODULUS (E): A material property describing its elasticity, $E = \frac{\sigma}{\epsilon}$

ACKNOWLEDGMENTS

I would like to thank Professor Blake Hannaford for his guidance and immense support of this research. His sage wisdom and advice has made this work possible. Additionally, I would like to thank Andrew Lewis whose invaluable perspective has always pointed me in the right direction. Lastly, I would like to thank my family and friends who have always been a constant source of support and encouragement.

DEDICATION

To N. K. Hwee, whose humility, sacrifice, and thirst for knowledge has inspired this work

Chapter 1

INTRODUCTION

1.1 Soft Robots

Soft robotics is a field of intrinsically soft mechanisms whose defining characteristic is its composition of high modulus materials such as silicone rubbers [39, 48]. These devices often are biologically inspired, mimicking skin, muscle tissues, an octopus' arm, elephant's trunk and many more [2, 6, 43]. Soft actuators are easy to actuate, often driven by fluidic pressure to bend or retract [39]. Their compliant bodies deform under load, absorbing the energy from a collision giving them an advantage in direct impact or blunt collisions making them ideal for human robot interaction and a collaborative or delicate workplace [39]. This compliance stems from nonlinear material properties, infinitely many degrees of freedom and large deflections under loading conditions [38]. However, these material properties also make soft manipulators extremely difficult to model accurately, and why they are not yet widely used in a commercial setting.

Soft robotics have many applications including locomotion and grasping. Due to their compliant bodies, soft robotics are ideal for locomotion in an unknown environment. They are capable of adapting to rough terrain, confined spaces and complex curvature without damaging the surface they are moving on [39]. Practical applications include pipe inspection and traversing rocky uneven terrain. Similarly, when used in a grasping setting, the soft manipulator will deform before damaging the object its grasping [37]. This is ideal for gripping objects with unknown geometries and delicate surfaces. These properties make soft manipulators ideal for surgery and pick and place of delicate objects. Surgical applications include laparoscopy where semi-rigid tools are necessary for moving tissue and other anatomical structures from obstructing the desired surgical site [37, 38].

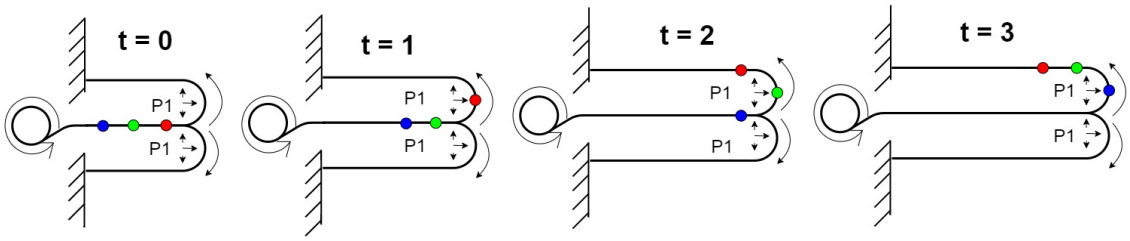

Figure 1.1: The eversion process is a method of tip growth: the tube lengthens with new material from within, the outer tubing remains stationary. Colored dots mark static positions along the tube body.

1.2 Eversion

Vine robots, or everted tubes, are a subclass of soft robots that grow in length by tip extension via eversion, where new material is pulled from within the tube and flipped inside out (Fig. 1.1). Lengthening by growth is bio-inspired, as are many soft robots, and is found in the roots of plants, growth of neurons, pollen tubes and sclerenchyma cells. All these organisms grow via tip extension [6].

Everted tubes are driven by a pressurized fluid, often air [6]. This type of growth makes everted tubes ideal for navigating convoluted tunnel-like environments because they grow along the path of least resistance, passively navigating through and around obstacles. Growth via eversion limits shear contact forces with the environment as the tube is able go grow without moving the body relative to the environment [34]. An additional benefit to pneumatic actuation is its inherent safety in hazardous environments, the soft robot body could not make sparks and ignite flammable gases [10]. Such exploration of hazardous environments might include inspection natural gas lines or pipes. Everted tubes have been demonstrated in search and rescue, medicine, and archaeology applications [10]. Previous studies have used eversion to minimize insertion forces of endoscopes in a colonoscopy phantom [40] and for patient-specific soft catheters for access to brain ventricles [42].

Everted tubes can be constructed from a variety of materials, including thermoplastics

(TPU, LDPE), Thermosets, Thermo-coated fabrics, Thermoset-coated fabrics, and uncoated fabrics [6]. Thermoplastics are the easiest to prototype, as they often can be purchased in manufactured tube shapes of multiple sizes and thicknesses. However, they have the lowest burst pressures and have been shown to fatigue quickly [6]. Fabricating tubes from thermoset-coated fabrics require a more involved manufacturing process; they must be sewn and sealed air-tight using adhesive. The structure of woven fabric prevents holes from rapidly propagating through the body, preventing bursting, making it ideal for navigating abrasive and rough environments [6]. An additional benefit of these light weight body materials is they maintain enough rigidity to support their own weight when spanning gaps [10, 22]

1.3 Everted Tube Kinematics and Modeling

Everted tubes have been modeled as inflated beams in many applications. Many studies have utilized the transverse and axial buckling equations derived in [12, 17] to model their behavior. They have also been used to compute smooth retraction forces [11] and describe kinetic wall interactions [21], and they have been validated in [20, 22, 31].

Many novel kinematic capabilities of vine robots have been recently developed, including active steering, smooth retraction, tip-mounted graspers, and dynamically reconfigurable joints [6, 10, 13, 16, 20, 22]. These works use of external devices along a robot's body to increases its operating workspace and capabilities. However, these rigid additions limit the robot's ability to squeeze through tight spaces since they cannot be crushed and re-inflated, thus hampering some of the benefits of the soft nature of everted tubes.

Greer *et al.* provide a differential kinematic model of the free growth of everted tubes. This algorithm accurately describes glancing and head-on growth around obstacles [19]. These kinematics have been extended by Haggerty *et al.*, who describe the kinetic interactions between an everted tube and wall. The reaction force will cause transverse buckling if the incident tube angle is greater than a theoretical minimum [21]. After a tube buckles from this transverse loading, it can freely grow along the wall while behaving like a hinge [21, 30]. In an environment with many obstacles, sections of tube between contact points behave as

independent beams [31]. Everted tubes have also been modeled as Cosserat Rods; Selvaggio *et al.* uses this model to determine the reachable workspace of an everted tube actuated by series Pneumatic Artificial Muscles (sPAM) [41]. This algorithm utilizes obstacles within the environment to increase the reachability of goal poses. Selvaggio *et al.* also used the closed-form solution of an externally loaded cantilever Cosserat rod to predict applied environmental forces on such obstacles [41].

1.4 Inflated Structures

Inflated structures have been used for decades to construct habitats, antennas, wings, and many more aerospace applications [45]. They are constructed of a skin material that holds load only when inflated. Larger structures are commonly a series of smaller tubular components sewn together to create complex shapes [45]. A beam bending model utilized in this thesis was developed by Comer *et al.* for the design of inflatable re-entry vehicles [12, 17, 30].

When under load, inflated beams exhibit some unique behaviors compared to standard beams. Wrinkles form near the root of the beam, and as the body material wrinkles, it no longer carries tension [12, 30, 45]. This is shown in Fig. 2.1 as the slack region. As the load increases, the slack region propagates around the beam, and θ_0 increases. As θ_0 approaches π, the beam will buckle and collapse, behaving like a hinge [30, 45].

1.5 Emergency Airway Management

Advanced airway management is a challenging and high-risk procedure critical to patient survival in many trauma settings. A patient who cannot breathe on their own may require advanced airway management where breaths are externally supplied through tubes expertly placed in their throat. These situations include cardiac arrest, stroke, drug overdose, loss of consciousness, and trauma including motor vehicle collision. Every year in the US nearly 350,000 people will experience Out of Hospital Cardiac Arrest (OHCA), and 90% of these patients will die [3]. Advanced airway management is critical in every OHCA situation to restore proper oxygenation to vital organs and prevent hypoxia [35]. Airway related injury is

the second highest cause of acute death among US combat fatalities [5,15]. The most common advanced airway management technique is EndoTracheal Intubation (ETI), where a trained professional inserts a plastic tube through the mouth and into the trachea to maintain an open airway. ETI is considered the "gold standard of airway management" [5,8]. Additional techniques include the Laryngeal Mask Airway (LMA), I-Gel, and CombiTube; these are large plastic devices inserted into the pharynx of the patient and seal inside the trachea or over the opening of the trachea [1, 5, 14, 15, 28, 35]. These devices require a significant amount of training and expertise to operate, and improper use often leads to death or long-lasting side effects such as spinal cord injuries, laceration, ischemia, and others [9, 33, 44]. These medical complications are usually caused by improper placement, forceful insertion, improperly sized devices, or cuff overinflation [33]. Studies show that user experience level is a key factor for first-pass success [24].

1.6 Insight and Motivation from King County Paramedics

Interviews were conducted with three King County paramedics to further understand emergency intubation in the field from professionals with first hand experience. These professionals hold positions as firefighter paramedics, a basic life support instructor for EMTs, and an intubation instructor at UW's paramedic training program. All paramedics were in agreement that ETI is the best solution in a trauma situation requiring advanced airway management. They list cardiac arrest, drug overdose, and physical trauma (ex. auto mobile collision) and the most common emergency situations requiring advanced airway management. In a cardiac arrest situation, according to multiple paramedics, if a patient's airway is not managed properly, even if resuscitated they will likely die. Proper ETI is ensures patient safety by establishing a *patent* airway. This is when the airway is completely sealed off, a small balloon is sealed within the trachea ensuring two things: air is supplied to the lungs, not the stomach, and that the airway is protected from aspiration and other fluids/secretions from entering it. Video laryngoscopes were developed to simplify the intubation process and were deployed with King County paramedics. They were quickly rejected because the camera

was easily occluded by blood and secretions from the airway rendering it useless. According to one paramedic, they were statistically less effective than standard laryngoscopes. All paramedics that were interviewed did not use SupraGlottic Airway (SGA) devices, such as an LMA or i-Gel, as they are easily dislodged from the airway. They require constant adjustment and attention to the airway during transit. The goal of emergency intubation is to safely transport a patient to the hospital. SGAs are also not usable if there is significant trauma to the airway, including a broken jaw, excessive blood, or swelling. In King County, this high risk and important procedure requires over 3,200 hours of training over two years to receive the required advanced life support training. As a result there are only 65-70 paramedics in King County and an EMT must arrive on the scene first and then call and wait for a paramedic to arrive.

Figure 1.2: An uninflated LMA

1.7 A Business Case for an Emergency Airway Device

The device outlined in this thesis is called EVBreathe, a standalone, automated device that can be placed in public areas that can be used by minimally trained users to save a life. Much

like an AED, EVBreathe will provide crucial patient support between a cardiac incident occurring and the arrival of paramedics. The author believes that everywhere there is a wall mounted AED, there should also be an EVBreathe device. There approximately 3.2 million AEDs in use and an estimated 70 million required to fully cover the US population [27]. This number would be a minimum number for EVBreathe as it has many more applications than a defibrillator. One potential pathway to commercialization is through the military. In 2021, the Defense Medical Research and Development Program solicited proposals for devices assisting in sustained resuscitation in a mass causality scenario. This is part of the Battlefield Resuscitation for Immediate Stabilization of Combat Casualties Award. This award seeks solutions that are low-weight, low-power, modular, portable and rugged and EVBreathe fits these requirements. Recall that airway related injury is the second highest cause of acute death among US combat fatalities [5, 15].

1.8 Academic Solutions to Emergency Airway Management

Several robot-assisted ETI systems have been developed. The Kepler Intubation System (KIS) uses a commercial laryngoscope mounted on a robot arm to perform teleoperated intubation [23]. An initial study of the KIS resulted in a 91% success rate in a clinical test. Remote Robot-Assisted Intubation System (RRAIS) is an over-the-mouth device for intubation that utilizes an endoscope to provide video feedback to its expert teleoperator [47]. RRAIS was slower to intubate porcine test subjects but held a higher success rate than manual laryngoscopy. The Robotic Endoscope-Automated via Laryngeal Imaging for Tracheal Intubation (REALITI) system partially automates the ETI procedure [4]. This system utilizes computer vision to identify the glottic entrance and automatically orients an endotracheal tube towards its geometric center using an actuator around the tube. Results showed that the REALITI system could assist non-medical professionals in performing laryngoscopy. While these systems made large strides to automate the intubation process, they largely depend on bulky, expensive, and specialized equipment or a highly trained teleoperator, limiting their widespread use for out-of-hospital emergencies.

1.9 Design of a Rotary Eversion Device

A rotary eversion base (Fig. 1.3) was adapted from `vinerobots.org` and by Hawkes *et al.* [22]. The everter capsule is used in all subsequent experiments and is constructed as follows. The soft robot body was spooled onto a spindle and released at a constant rate by a DC motor with encoder feedback. The spindle has a through-hole allowing the Semi-Rigid Air Delivery Tube to be routed out of the pressure vessel. It is connected to a pneumatic rotary union (Mosmatic, Bristol, WI) to prevent kinking.

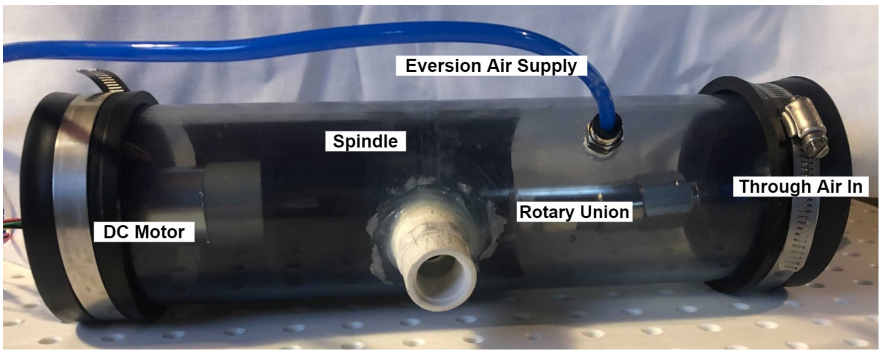

Figure 1.3: Motor controlled rotary eversion assembly with novel rotary union for external access to internal lumen.

Pneumatic Control System

Pneumatic pressure is supplied by a 12V DC peristaltic pump with a manual pressure regulator (Omega, AR91-015) and a 2L pneumatic tank to act as a pressure filter. Pressure is measured with a gauge pressure transducer (Honeywell, SSCDANN150PG2A3). Data was filtered using a four (4) frame moving average. A diagram of the overall control system is shown in figure 1.4.

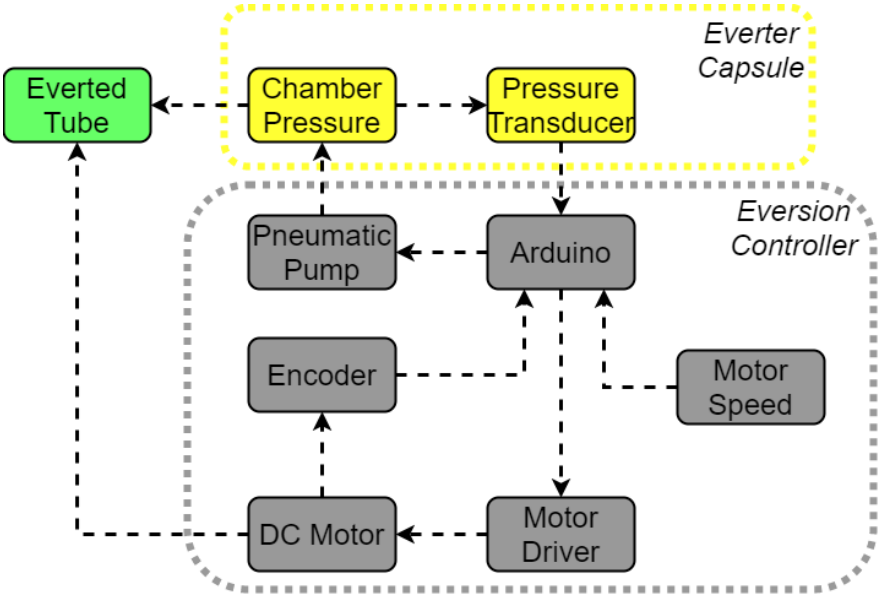

Figure 1.4: Pneumatic Control Diagram of Everter

1.10 Contribution

The contributions of this thesis are as follows:

- A validation of an inflated beam model applied to everted tubes.
- A method to determine an everted tube's tip pose from static positions in the environment.
- A novel everted balloon construction applied to emergency airway management.
- A method for supplying air through the internal lumen of an everted tube

Chapter 2

A METHOD FOR EVALUATING AN INFLATED BEAM MODEL APPLIED TO EVERTED TUBES

This chapter will demonstrate a method for solving the beam model introduced by Comer *et al.* This solution will be used to compare the performance of straight and everted cantilever beams under three different variable loading conditions and validate that everted tubes can be modeled as inflated beams. Current everted tube research uses the maximum axial and transverse loading conditions outlined by [12, 17] but have not validated beam deflections or curvatures at loads less than critical loading conditions [20, 21, 31]. Beam deflection was also used to determine an everted tube's curvature, which we have extended to estimate everted tube pose from environmental interactions. Selvaggio *et al.* estimated this pose using an externally loaded cantilever Cosserat rod for an everted tube with actuation along the length.

2.1 Solving an Inflated Cantilever Beam

This thesis uses the model developed by Comer *et al.* for an inflated cantilever beam with a length much greater than its radius [12]. The beam model, as applied to an everted tube, is shown in figure 2.1. The curvature

$$\frac{d^2y}{dx^2} = \begin{cases} \frac{Qx}{EtR^3\pi} & 0 < x < \frac{\pi pR^3}{2Q} \\ \frac{Qx}{EtR^3}\frac{2}{2\pi - 2\theta_0 + sin(2\theta_0)} & \frac{\pi pR^3}{2Q} < x < L \end{cases} \tag{2.1}$$

describes the vertical displacement within the wrinkled and unwrinkled region of the beam. x is the distance along the beam measured from the tip, Q is the applied tip load, E is the Young's Modulus of the material; R is the beam's radius, and t is the material thickness. It is important to note that the origin of the beam is defined at the free end, shown in Fig. 2.1, where the load is applied. Displacement downwards is defined in the positive y direction.

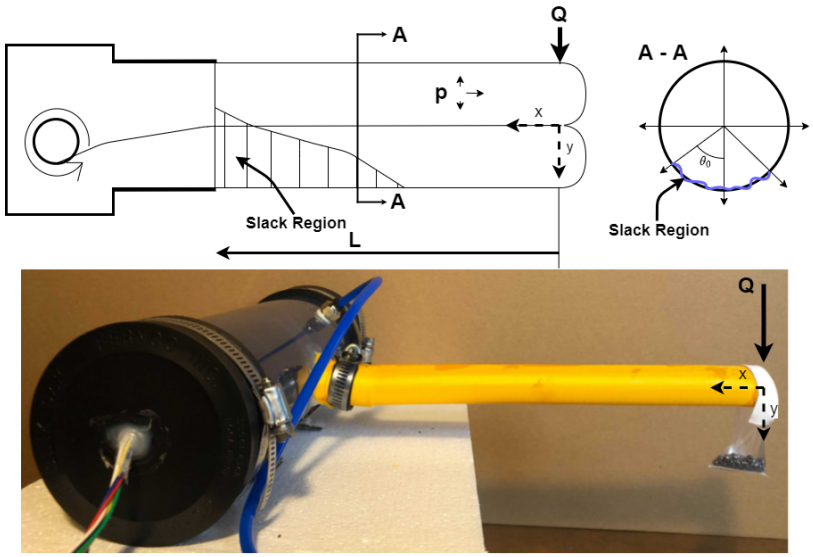

Figure 2.1: *Top:* An everted cantilever beam with length, L; internal pressure, p; and external load, Q. Note the coordinate frame is centered at the tip of the beam. *Bottom:* An everted silicone coated nylon beam carrying a cantilevered tip load.

This curvature equation is similar to the standard cantilever beam equation of $\kappa = \frac{M}{EI}$, where the inertia of a thin-walled cylinder is $I = \pi R^3 t$. θ_0 is the wrinkle angle around the beam, shown in figure 2.1. Wrinkle angle is numerically approximated from eq. 2.2 using a 5^{th} order polynomial and is described as function of $\frac{Qx}{pR^3}$, eq. 2.5. This process is outlined by [45] and shown in Fig. 2.2.

$$\frac{Qx}{pR^3} = \frac{\pi(2\pi - 2\theta_0 + sin(2\theta_0)}{4[sin(\theta_0) + (\pi - \theta_0)cos(\theta_0)]} \tag{2.2}$$

The problem is simplified by non-dimensionalizing the position in the x and y direction:

$$\xi = (\frac{Q}{pR^3})x, \tag{2.3}$$

$$\eta = (\frac{Q^2 Et}{p^3 R^3})y. \tag{2.4}$$

$$\theta_0 = f(\frac{Qx}{pR^3}) = f(\xi) \tag{2.5}$$

gives the expression for curvature:

$$\frac{d^2\eta}{d\xi^2} = \begin{cases} \frac{\xi}{\pi} & \frac{\pi}{2} > \xi > 0 \\ \xi\frac{2}{2\pi - 2\theta_0 + sin(\theta_0)} & \pi > \xi > \frac{\pi}{2} \end{cases}. \tag{2.6}$$

We solve the beam by decomposing the non-dimensional model into a system of first order equations by η_1 and η_2, where $\eta_1 = \eta,\ \eta_2 = \frac{d\eta}{d\xi}$:

$$\frac{d}{d\xi}\begin{bmatrix}\eta_1 \\ \eta_2\end{bmatrix} = \begin{bmatrix} \eta_2 \\ \begin{cases} \xi\frac{2}{2\pi - 2\theta_0 + sin(\theta_0)} & \pi > \xi > \frac{\pi}{2} \\ \frac{\xi}{\pi} & \frac{\pi}{2} > \xi > 0 \end{cases} \end{bmatrix}. \tag{2.7}$$

Using the initial conditions described in [12] a solution can be found. The initial conditions are that the displacement and slope at the root ($x = L$) of the beam are both zero. The system is solved by numerically solving the initial value problem backward, simulating from $x = L$ to $x = 0$. Matlab's ODE solver function, ode45, was used to solve

$$\eta(\xi(L)) = 0, \quad \frac{d\eta(\xi(L))}{d\xi} = 0$$
$$\xi(L) = \frac{QL}{pR^3}.$$

2.2 Materials Selection and Testing

Two different beam materials were used to validate the inflated beam model: Silicone Coated Nylon (Seattle Fabrics, Seattle, WA, USA) and 2.54 cm diameter with 2mil (0.05mm) wall thickness Low-Density-PolyEthylene (LDPE) tubing (ULINE, Pleasant Prairie, WI, USA). The Silicone Coated Nylon had a measured thickness of 0.12 mm. Beams were sewn to a 2.54 cm diameter and sealed using Seam Grip WP (Gear Aid, Bellingham, WA, USA). The

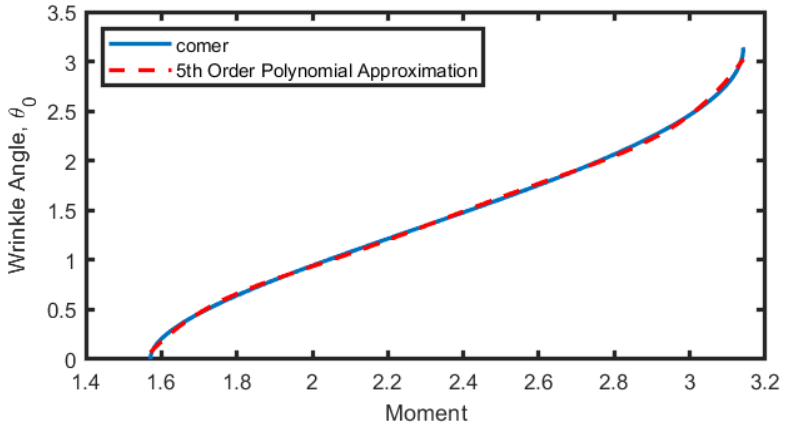

Figure 2.2: 5^{th} order polynomial approximation of wrinkle angle as a function of moment

LDPE tubing held a significant amount of memory from its manufacturing and storage on a large reel, giving all inflated tubes a nominal curvature. To eliminate the curvature in the plastic was annealed by hanging vertically and stretched by weights in a sunny enclosed patio.

Each material was tensile tested, the stress and strain were computed using a video extensometer and digital image correlation. Materials were stretched at a rate of 5mm/min. Both annealed and un-annealed LDPE samples were tested to ensure that the annealing process did not affect the mechanical properties of the plastic. The Young's modulus was measured between the maximum and minimum stress within the beam during the following conditions: length of 0.357 m, internal pressure of 10.34 kPa, and applied tip load of 0.155 N. The minimum stress is the longitudinal stress of a pressure vessel and the maximum axial stress at the root of the loaded cantilever beam ($x = L$), outlined in [12]:

$$\sigma_m = \frac{QL}{tR^2} \frac{2(1 + cos(\theta_0))}{2\pi - 2\theta_0 + sin(2\theta_0)}. \tag{2.8}$$

2.3 Parameter Variation

The model was validated by comparing the tip deflection of straight and everted tubes. Straight tubes are defined as traditional cylindrical thin-walled inflated beam. In contrast everted tubes have an inner lumen, or tail, connecting back to the spindle, shown in Fig. 2.1. Tests varied the independent values of eq. 2.4: beam length (L), internal pressure (p), and external load (Q). Silicone coated nylon and annealed LDPE were the two tube materials used. The tip displacement is $y_d = \eta \frac{p^3 R^6}{Q^2 E t}$ for $\xi(L)$. Transverse buckling occurred when the beam collapses to the floor under the test conditions.

For beams under variable tip load, a 0.368 m beam with a 1.27 cm radius and 10.34 kPa internal pressure was loaded at the tip by weights of increasing mass. The tip displacement was measured between every increase in weight, the weight was also removed between increases. The beam was loaded until it experienced transverse buckling and collapsed. Collapse conditions were compared to the theoretical critical values [12]:

$$Q_{max} = \frac{\pi p R^3}{L} \tag{2.9}$$

A new plastic beam was used after each collapse to avoid fatigue and plastic deformation between trials. Because the nylon had a significantly higher stiffness, beams were depressurized and re-oriented after every collapse to mitigate any seam dependent deflection.

Everted and straight beams of variable length were evaluated by pressurizing to 10.34 kPa and tip loading with a 0.155 N, tip deflection was measured. This process was repeated for beams of increasing length until the beam collapsed under load. Beams were similarly replaced or re-oriented after each collapse. Collapse conditions were compared to the theoretical max length.

Beams of varying internal pressure were also evaluated using a constant length of 0.357 m and mass of 0.155 N. The tube's internal pressure was decreased from 27.58 kPa until collapse occurred. All beams were depressurized and unloaded between each trial. Eq. 2.9 was used to determine additional critical buckling conditions, max length (L_{max}) and

minimum internal pressure (P_{min}).

2.4 Curvature Evaluation

Annealed LDPE everted beams of variable length, and constant pressure of 10.34 kPa were loaded with a 0.155 N tip load. Each beam was marked with a series of black dots at 2.54 cm increments. Images were taken before and during loading. Their relative vertical displacement was measured using an image mask in Matlab (Fig. 2.3). Displacement at discrete locations along the beam was compared with the inflated beam model. The tip slope was determined from the two distal-most markers and compared with the modeled beam slope, η_2, at the tip.

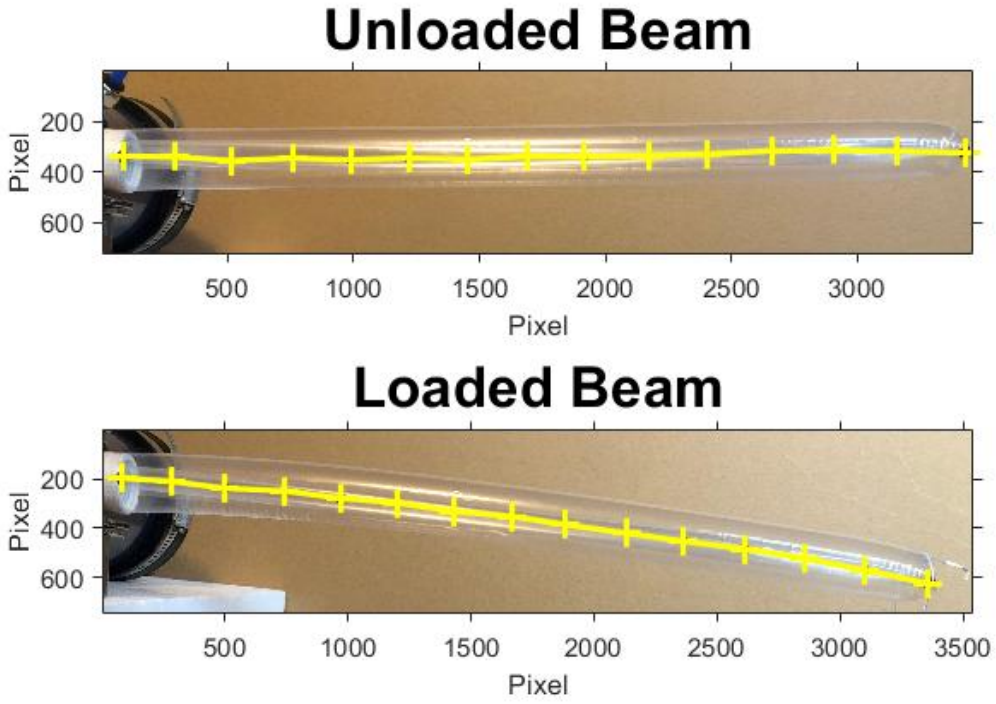

Figure 2.3: Everted inflated cantilever beam with and without a tip load. An image mask was used to determine the centroid of each marker to determine relative displacements along the beam.

2.5 Curvature Estimation from Environmental Interactions

The model was used to predict tube curvature from environmental interactions, shown in Fig. 2.4. An annealed LDPE everted tube was tip-displaced a fixed amount. Given constant parameters of length and internal pressure, the theoretical load at the tip was be iteratively determined, and the curvature estimated from the model. A tube with tip displacement greater than the theoretical maximum was modeled as buckled, and the curvature was be approximated as a straight line between tip and base, as presented in [31].

Figure 2.4: An LDPE everted beam deflected a fixed amount

Chapter 3

RESULTS AND IMPLICATIONS FOR MODELING EVERTED TUBES AS INFLATED BEAMS

3.1 Material Properties

Annealed and non-annealed LDPE samples were loaded to between 10% and 12% strain, shown in Fig. 3.1. The Young's Modulus was determined from the elastic region, $< 2\%$ strain, to be 199 MPa and 243 MPa for the non-annealed and annealed samples, respectively. All subsequent simulations use the average across all LDPE conditions, 227 MPa. The Young's Modulus of silicone coated nylon was linear within the max/min stress region, consistent with [30], and measured to be 495 MPa.

3.2 Results: Variable Tip Load

A constant length, constant pressure, cantilever beam under variable tip load was tested. The results are shown in Fig. 3.2 which plots measured tip deflection against applied tip load. A solid blue line shows the theoretical tip deflection until the theoretical buckling condition and displacement. Absolute error was calculated as the difference between the model and measured tip deflection at a specific load. Beam collapse conditions are shown with $\square$ and $\triangle$ markers and evaluated as a percentage of the theoretical maximum load condition. Buckling displacement is the measured tip deflection at the loading condition just before the experimental buckling condition. Everted and straight nylon beams had average absolute tip deflection errors of 19.3 and 16 mm, respectively. The everted beams collapsed at 88% of the theoretical maximum load, while the straight tubes collapsed at 107% of the theoretical maximum. The LDPE tubes had a lower absolute tip deflection error of 2.2 and 3.8 mm for everted and straight tubes, respectively. On average, everted LDPE beams

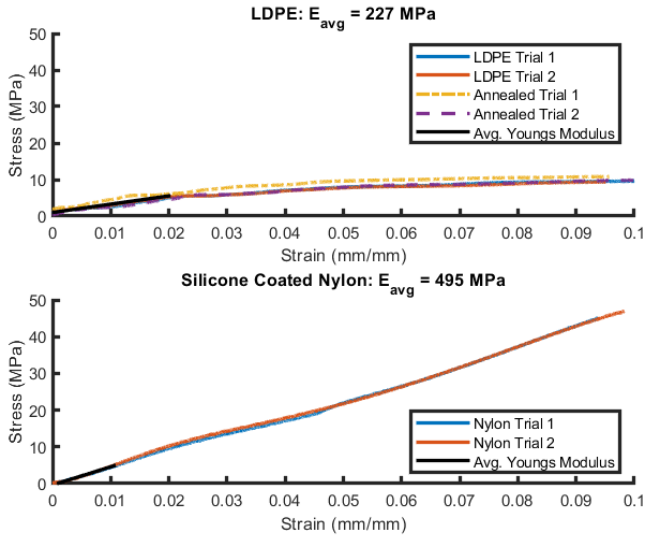

Figure 3.1: Stress-strain performance of the tested materials. *Top:* LDPE results, a comparison between the annealed and unannealed material shows approximately the same Young's modulus of 227MPa. *Bottom:* Silicone coated nylon was strained up to 10%, the data shows that this is still in the elastic region. The Young's Modulus was calculated within experimental stress values.

collapsed at 80% of the theoretical maximum load at an average displacement of 0.039 m (SD: 7 mm). Straight LDPE beams collapsed at 106% of the theoretical maximum load at an average displacement of 0.056 m (SD: 5 mm). The theoretical maximum displacement at Q_{max} is 0.088 m.

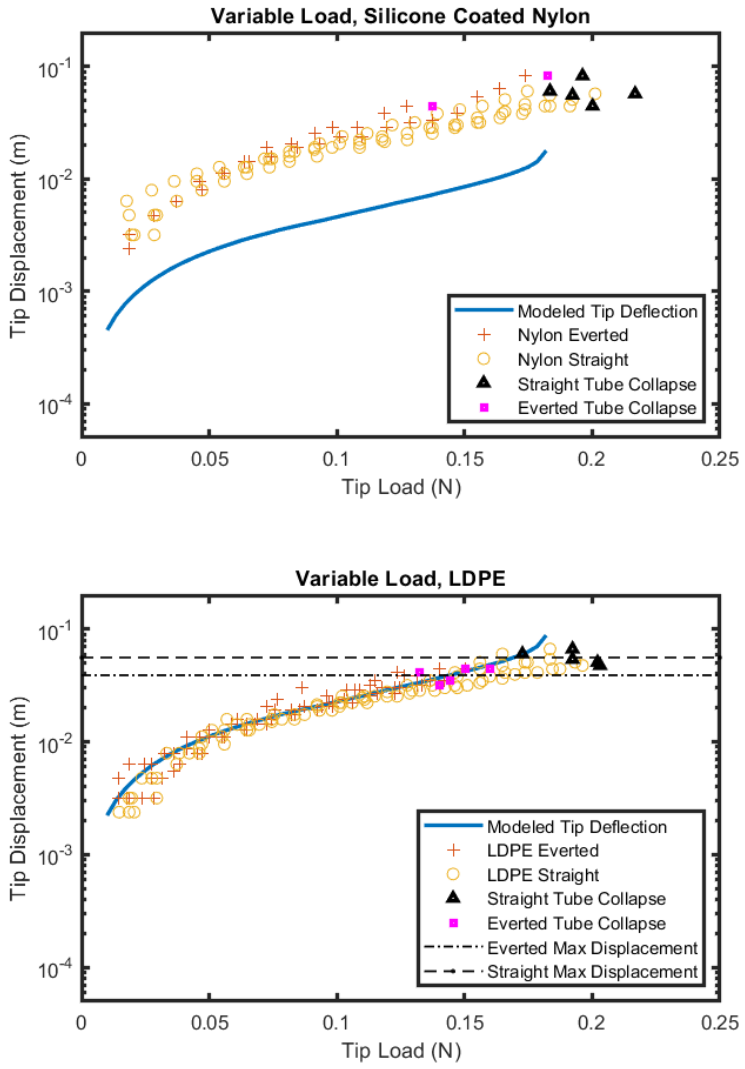

Figure 3.2: Tip deflection of straight and everted inflated beams under variable load at a constant length of 0.357 m and constant pressure of 10.34 kPa. The □ and △ markers represent the load at which the beam collapsed. *Top:* Silicone coated nylon beam. *Bottom:* Annealed LDPE beam.

3.3 Results: Variable Beam Length

A constant pressure, constant load cantilever beam with variable length was tested. The results are shown in Fig. 3.3 which plots measured tip deflection against beam length. A solid blue line shows the theoretical tip deflection until the theoretical buckling length and displacement. Absolute error was calculated as the difference between the model and measured tip deflection at a specific beam lengths. Collapse conditions are shown with □ and △ markers and evaluated as a percentage of the theoretical maximum length. Buckling displacement is the measured tip deflection at the beam length just before the experimental buckling length. Everted and straight nylon beams had absolute tip deflection errors of 12.9 and 8.3 mm, respectively. The everted beams collapsed at 88% of the theoretical maximum load, while the straight tubes collapsed at 106% of the theoretical maximum. The LDPE tubes had lower absolute tip deflection errors of 2.5 and 8.6 mm for everted and straight, respectively. Everted LDPE beams collapsed at 77% of the theoretical maximum load at an average displacement of 0.029 m (SD: 4 mm). Straight LDPE beams collapsed at 102% of the theoretical maximum load at an average displacement of 0.054 m (SD: 3 mm). The theoretical maximum displacement at L_{max} is 0.119 m.

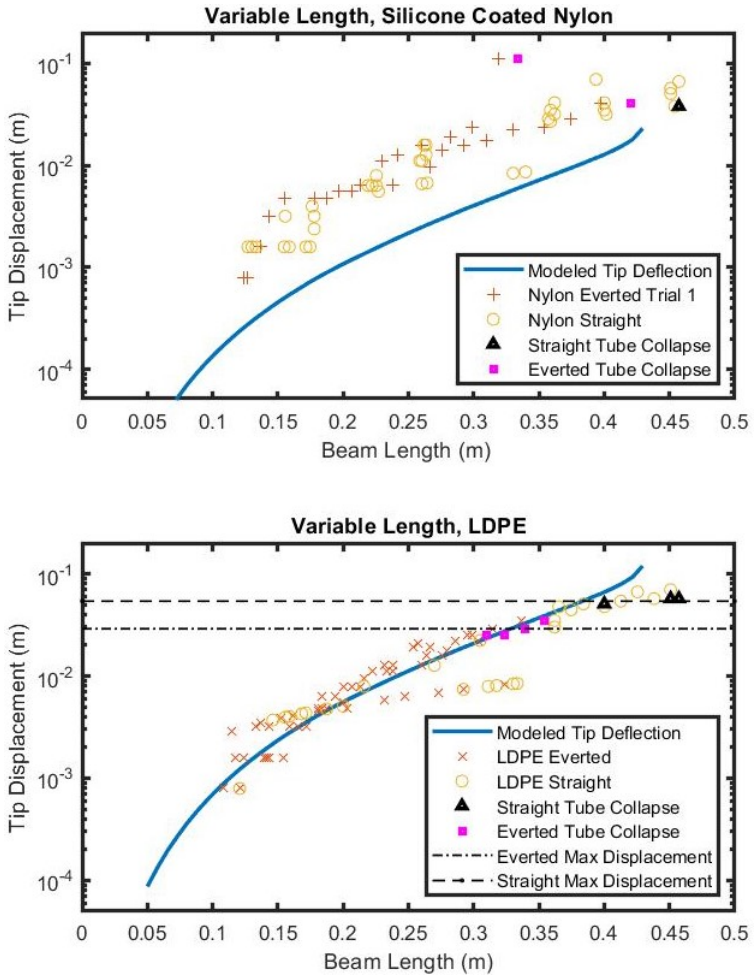

Figure 3.3: Tip deflection of straight and everted beams under constant 15.8 g load, pressurized to 10.34 kPa under variable lengths.The □ and △ markers represent the load at which the beam collapsed. *Top:* Silicone coated nylon beam. *Bottom:* Annealed LDPE beam.

3.4 Results: Variable Pressure

A constant load, constant length cantilever beam with variable internal pressure was tested. The results are shown in Fig. 3.4 which plots tip deflection against internal pressure. A solid blue line shows the theoretical tip deflection from the theoretical minimum internal pressure to the deflection at 30kPa. Absolute error was calculated as the difference between the modeled and measured tip deflection at a specific internal pressure. Collapse conditions are shown with □ and △ markers and evaluated as a percentage of the theoretical minimum pressure. Buckling displacement is the measured tip deflection at the internal pressure just before the experimental buckling pressure. Everted, and straight nylon beams had an absolute tip deflection error of 29.1 and 12.9 m, respectively. Nylon everted beams, on average, collapsed at 116% of the theoretical minimum pressure while the straight beams collapsed at 93% of the theoretical minimum. LDPE tubes had a lower absolute tip deflection of error of 9.3 and 8.2 mm for everted and straight beams, respectively. The everted LDPE beams collapsed at 120% of the theoretical minimum pressure at a displacement of 0.038m (SD: 1 mm). Straight beams collapsed at 77% of the theoretical minimum at a displacement of 0.034m (SD: 1 mm). The theoretical maximum displacement at (P_{min}) is 0.0747m.

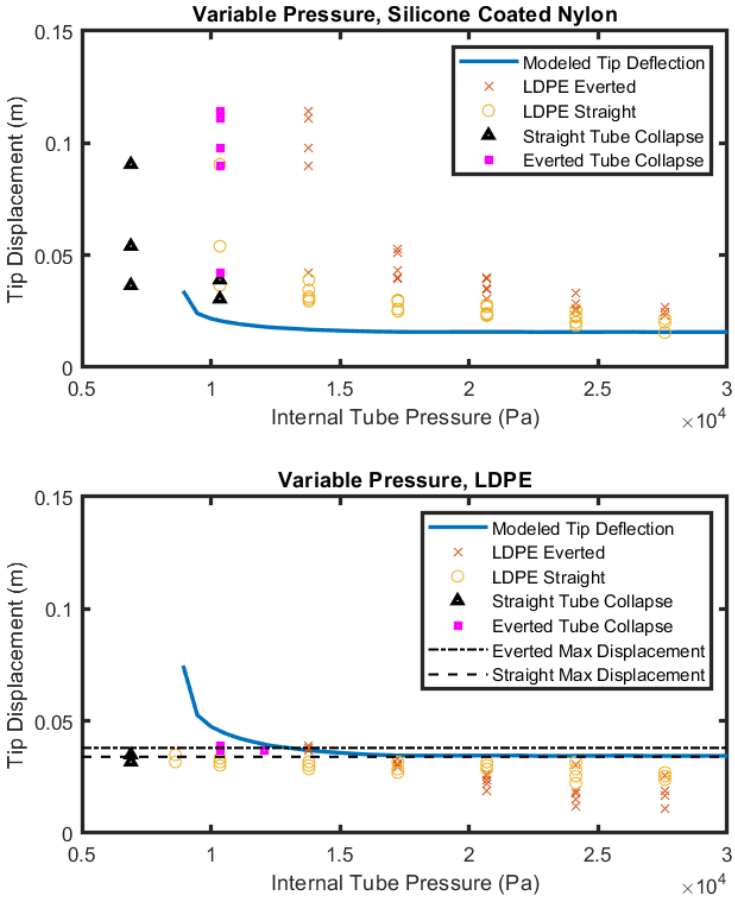

Figure 3.4: Tip deflection of straight and everted beams of variable pressure under constant 0.155 N load and length of 0.357 m. The □ and △ markers represent the load at which the beam collapsed. *Top:* Silicone coated nylon beam. *Bottom:* Annealed LDPE beam.

3.5 Results: Curvature Under Load

The curvature of an everted cantilever beam of variable length is shown in Fig. 3.5. The origin is located at the tip of the beam, and the plot shows distance from the tip against relative displacement. The absolute displacement error was computed as the difference the measured vertical displacement and modeled vertical displacement at discrete locations along the length of the beam. The average displacement error was computed to be 1.1, 1.5, 2.6 and 4.9 mm for beams of length 0.254, 0.305, 0.330, and 0.356m. While the absolute error increases with beam length, the relative tip displacement error is 14%, 11.8%, 12.4%, and 18.5%. The tip slope error, $\frac{dy}{dx}$, was measured to be 0.011, 0.017, 0.012, and 0.02 rad for the given lengths.

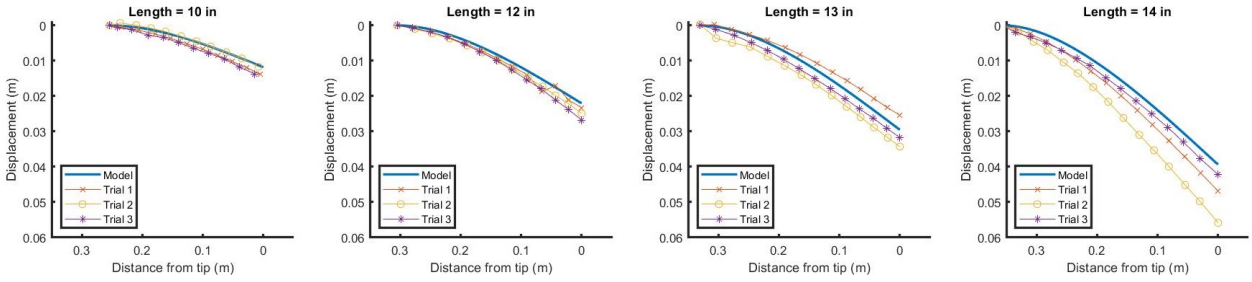

Figure 3.5: Modeled and measured curvature for everted LDPE beams of length 0.254, 0.305, 0.330, and 0.356 m. Each beam was under a 0.155 N load and pressurized to 10.34 kPa.

3.6 Estimating Curvature from Environmental Obstacles

An inflated beam's curvature was estimated from a known tip displacement by iteratively solving for the theoretical applied load, given constant beam parameters. Absolute error was calculated from the difference between the estimated curvature and the measured curvature. Figure 3.6 shows the beams interaction with an obstacle relative to its nominal unloaded position. For tip displacements of 17, 21, and 34 mm an absolute error of 0.7, 0.7, and 0.9 mm and relative error of 20%, 17% and 15% was calculated, respectively. The curvature of beams displaced greater than their theoretical max, determined using eq. 2.9, were be modeled as a straight line between the tip and base. This straight-line approximation of buckled beams recorded average absolute errors of 1.1 and 1.4 mm and relative error of 4.5% and 3%.

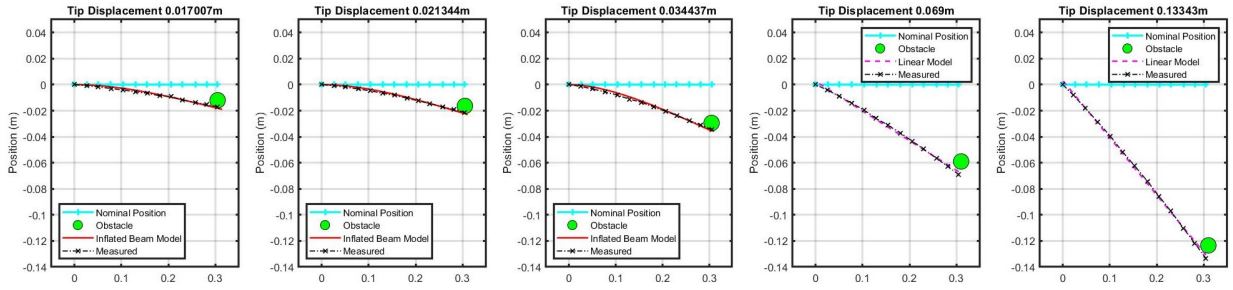

Figure 3.6: A comparison of the modeled and measured curvature for beams deflected by an obstacle in the environment. A beam 0.305 m in length and pressurized to 10.34 kPa was deflected to a known distance. Its curvature was measured using a series of markers spaced 2.54 cm apart. Given the tip displacement, length, and pressure, the applied force and curvature were estimated.

3.7 Discussion: Tip Deflection

The deflection model provided by Comer *et al.* best fit the tip deflections of the annealed LDPE tubes with an average tip deflection error of 6 mm for both straight and everted beams. The measured tip deflection of silicone coated nylon did not match the magnitude predicted in the model with an average tip deflection error of 16.4 mm for both straight and everted beams. The model held the same shape as the experimental tip deflection data. In this cantilever application, modeled nylon tubes exhibited an effective stiffness of approximately 25% of the measured value. The data shows that $E_{model} = .25E_{longitudinal}$, where $E_{longitudinal}$ is the Young's Modulus computed from the tensile test. This is likely due to the direction of the applied load on the weave pattern of the nylon. Silicone coated nylon can be thought of as a composite material whose Young's Modulus is not constant with respect to the angle of the applied load. Tensile testing yielded the stiffness in the longitudinal direction. Cantilever loading applies transverse stress on the beam, a loading condition where $E_{transverse} < E_{longitudinal}$. For a structure where the load may be applied in an arbitrary direction with respect to the weave, performance consistent with the maximum material properties determined from longitudinal testing cannot be expected.

In all cases, the everted and straight tubes showed approximately the same tip deflection throughout each experiment. Although in all experiments, everted tubes collapsed at conditions before the theoretical max/min and straight tubes collapsed after. Across all experiments, everted nylon tubes buckled 86% of the theoretical buckling condition while everted LDPE tubes collapsed at 79% of the theoretical buckling condition. On average, straight nylon tubes buckled at 107% of the theoretical buckling condition and straight LDPE tubes collapsed at 110% of the theoretical buckling condition. This could be due to wrinkles or fatigue generated in the material during the eversion process. Recall that as $\lim_{\theta_0 \to \pi}$ the beam collapses [45]. It is possible that material creasing during eversion contributed wrinkle propagation when under load. The deflection of an inflated cantilever beam model is valid for homogeneous materials such as LDPE. The modeled beam's deflection held true until

near collapse, but the collapse condition may not be accurately determined by the model. A beam's collapse may be defined better by a maximum displacement. Across all LDPE tests, beams collapsed at a consistent displacement rather than load. In nearly all conditions, everted tubes collapsed at a smaller displacement than straight tubes.

3.8 Discussion: Curvature Validation

The curvature of an everted tube was validated using both a transverse gravity load and external lateral displacement. Tubes under a transverse gravity load had a relative tip displacement error of 14.2%, and tubes under an external lateral displacement had a relative curvature error of 17.3%. Tubes externally displaced greater than the theoretical maximum were approximated as a straight line and showed an error of 3.75%. Longer tubes showed greater absolute tip displacement error but all beams had similar relative tip error. Tip slope computation showed a similar error trend across beams of variable length. The accuracy of this value can be increased by increasing the quality of the image tracking system. Predicting curvature from environmental displacements implies that the model may be used to accurately estimate interaction forces with the wall given a specific tip deflection. Allowing a user to determine applied forces in a known sensitive environment such as an archaeological dig site, [10], or within the body [40, 42].

3.9 Applications: Pose Estimation from Environment

The static pose of the tip of an everted tube can be estimated using tip deflection. The tip reference frame is calculated using the differential kinematics model derived by [19]:

$$\dot{\vec{p}} = u\frac{||\vec{p} - \vec{c_n}||}{\hat{t} \cdot (\vec{p} - \vec{c_n})} \tag{3.1}$$

Given an obstacle within an environment, tip translation is determined by :

$$^{\vec{c_n}}\mathbf{t}_{\vec{p}} = \vec{p}, \tag{3.2}$$

where $\hat{t}$ is the unit vector parallel to the surface of the obstacle, u is the eversion growth rate, $\hat{p}$ is the tip location, and c_n is the nearest contact point. In the case of Fig. 3.7 c_n

is the everter base. The curvature at the tip or heading, η_2 when $\xi = 0$, gives the rotation angle of the tip coordinate frame:

$$^{\vec{c_n}}\mathbf{R}_{\vec{p}} = \eta_2 \frac{p^2 R^3}{QEt} \tag{3.3}$$

From tip translation and tip slope, a planar and homogeneous transformation matrix can be determined. This process is similarly computed in Selvaggio *et al.* [41], where the everted tube is modeled as a Cosserat rod. Forces applied to the obstacle can also be computed from the pose.

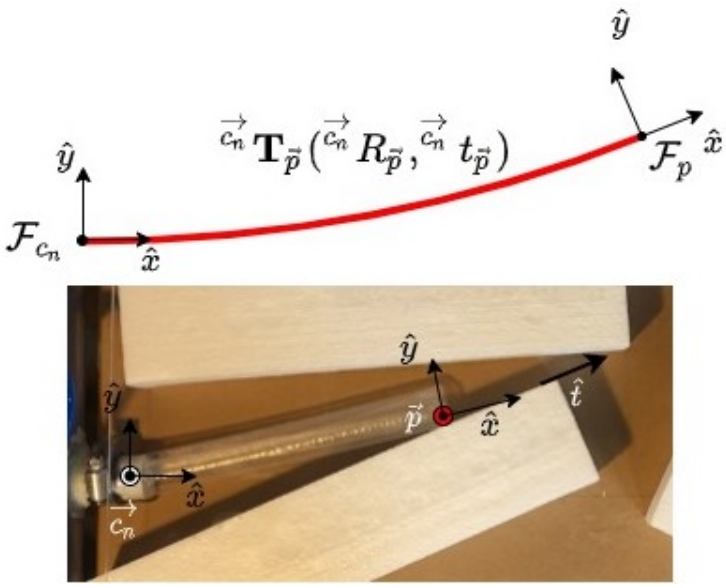

Figure 3.7: Tip pose estimation from static tip deflection

3.10 Applications: Extension of Current Kinematic Modeling

Understanding the static behavior of everted beams will help give insight into their kinematic behavior. This work can support the algorithms derived in several published works.

Tip slope angle could also be useful in determining transverse buckling while growing along a wall. If a tube is incident to a wall at an angle greater than he minimum incident angle described by Haggerty *et al.* [21], transverse buckling occurs and the tube grows along

the wall. If a tube is incident to the wall at an angle less than the determined minimum incident angle, the static beam will bend according to the model described by [12] and will behave as shown in Fig. 3.6. In this instance, tip slope angle should be considered when computing incident angle. Transverse buckling may occur when tip slope is considered. This insight could help understand a tube's kinematic behavior very close to buckling conditions.

Retraction without buckling of an everted tube is greatly influenced by the tube's curvature [11]. The curvature model derived in this paper can provide an analytical solution to assist in computing retraction forces.

Everted tubes in previous path planning algorithms have been modeled as straight lines between obstacles and discrete pivot points [19]. The inflated beam model allows for the beam's curvature to be computed and included in these kinematic models.

Chapter 4

THE DESIGN AND VALIDATION OF AN EMERGENCY AIRWAY DEVICE

We propose a novel, multi-element, everted tube designed to deploy into a patient's throat and safely establish a sealed airway. In emergency settings, a reliable, compact, fully automated device is needed to simplify advanced airway management and make it available for bystander intervention. A vine robot is proposed because it can reliably navigate the curvature of airway anatomy without complex control algorithms. The length and linear growth rate are controlled by motor feedback. But tube heading is uncontrolled as the tube grows into the patient's throat, allowing it to passively enter the trachea or seal around it.

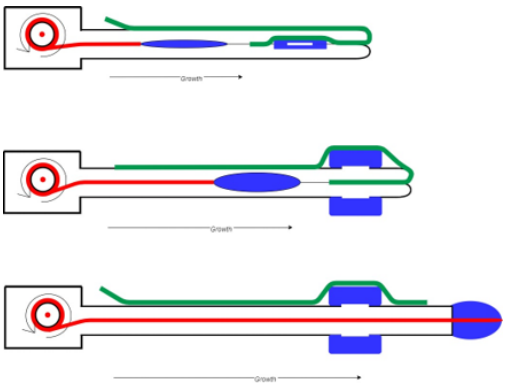

Figure 4.1: The deployment of the proposed dual-balloon (blue) and dual-air delivery. The red tube marks the inner lumen deployed in series and the green marks the outer tube deployed in parallel.

Novel balloon configurations will seal the airway to enable ventilation through co-deployed, semi-rigid tubes. Dual balloon construction (Fig. 4.4 Config 4) allows for the tube to deploy

into the patient's esophagus or trachea and deliver air safely to the patient through one of two air supply lines incorporated on the everted tube (Fig. 4.2). This design is inspired by the CombiTube, which is also intended to be safely inserted into the trachea or esophagus [1,29]. It has lost favor with emergency responders due to its large size. This dual-option construction aims to solve two potential misuses of other manual devices: improper insertion of endotracheal tubes or LMA like devices into the esophagus and insufficient sealing of the airway. In both cases, patients may not receive adequate ventilation [36, 46].

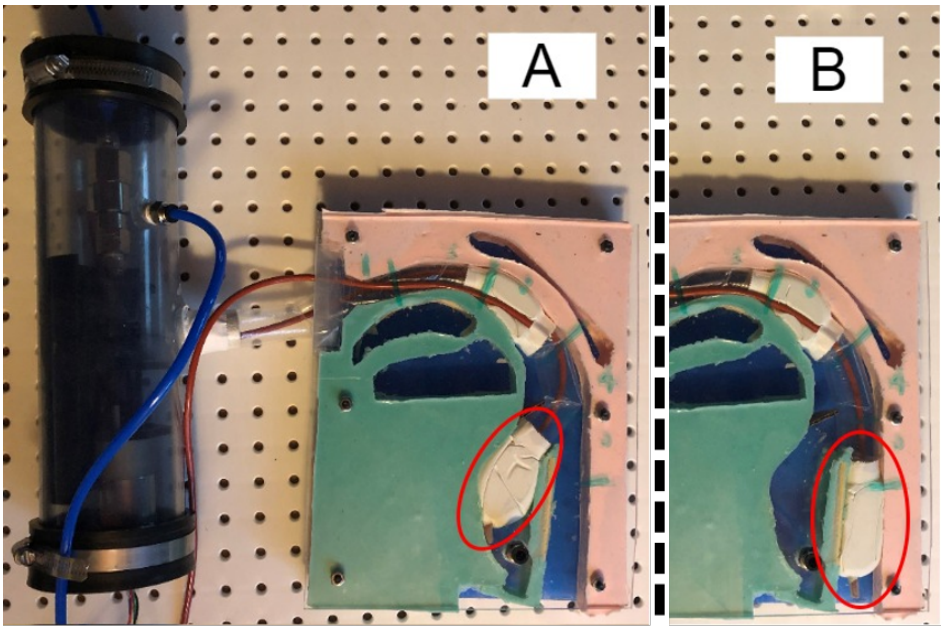

Figure 4.2: Deployment of novel multi-element everted tube. Dual balloons ensures air delivery to the patient if deployed into trachea or esophagus. [A] Tube in trachea: breathing air is supplied through internal lumen running through the tip balloon. [B] Tube in esophagus: tip balloon seals off stomach, preventing gastric inflation, and breathing air is supplied through external lumen deployed parallel to soft body tube.

Figure 4.2 shows the proposed tube construction and its final deployment in the airway. If the tube lodges in the upper esophagus, the tip balloon will seal off the esophagus, preventing

air from entering the stomach. Pulmonary ventilation is delivered from the side air delivery tube deployed in parallel with the soft body tube. The seal established by the proximal cuff balloon will prevent air from escaping through the mouth or nose. If the tube lodges in the trachea, the tip balloon will seal against the upper tracheal mucosa in the same manner as a standard endotracheal tube cuff. Pulmonary ventilation will be delivered to the patient using the inner air delivery tube that passes through the tip balloon.

The inner air delivery tube is connected in with the soft robot body, deploying in series behind the body tube. A channel in the spindle allows for the inner air tube to be routed out of the device. A rotary pneumatic union is used to prevent kinking caused by spindle rotation and has not been demonstrated in other everted tube applications. This is shown in fig. 4.1.

The side air delivery tube is deployed in parallel with the soft body tube and can be considered a payload of the everted tube. Parallel payload deployment along an everted tube has been used to deploy and actuate series pouch motors for heading control [6, 10].

4.1 Airway Phantom Design and Construction

A CT scan of a healthy teenage male was used to construct a simplified airway phantom (Fig. 4.5). The 2x scaled airway phantom with a constant depth of 2 cm was cast using an approximated outline of the airway, Fig. 4.3. It was scaled to match the size of commercially available 2.54cm diameter tubing such that the anatomy and tube had roughly the same cross-sectional area. Silicone with durometers 20 and 15 was used (Mold Max 20 and Mold Star 15) to simulate the soft tissues of the airway. Air pockets were left in the phantom at the soft palate and the tongue to approximate highly compliant tissues. The esophageal sphincter was modeled as open and does not reflect the normally closed nature of the esophagus. A single DOF epiglottis was modeled using a torsion spring to approximate the torque, 0.05 in-lbs, required to depress the epiglottis [25].

Figure 4.3: Male molds for casting silicone phantom

4.2 Soft Robot Body and Design of Novel Balloon Construction

This study will evaluate the performance of proposed elements in the following configurations:

1. Tip balloon, inner semi-rigid tube air delivery
2. Cuff balloon, inner semi-rigid tube air delivery
3. Cuff balloon, side mounted semi-rigid tube air delivery
4. Tip and cuff balloon, side mounted semi-rigid tube air delivery

Soft Robot body

The everted tube body is composed of: **Soft Body Tube** - thin LDPE tubing (ULINE), 1" diameter and 2mil (0.05mm) wall thickness; **Semi-Rigid Air Delivery Tube** - 3mm ID x 4mm OD latex tubing (Uxcell); and **Airway Sealing Balloons** - 9" latex balloons fixed to the soft body tube with J&J Waterproof tape.

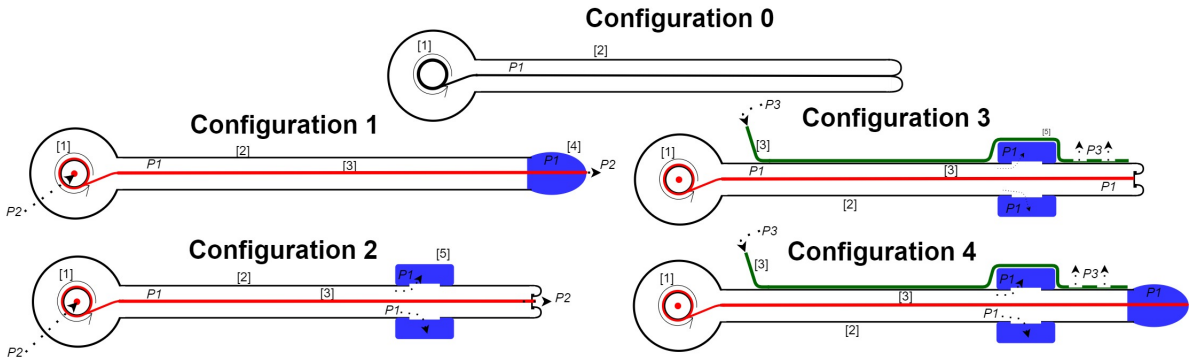

Figure 4.4: Multi-element everted tube. (1) Eversion Base (2) Soft Body Tube (3) Semi-Rigid Air Delivery Tube (4) Tip Balloon (5) Cuff Balloon

4.3 Device Evaluation and Testing

Each element of the proposed device was constructed as an independent everting device to characterize its effect on an integrated system. Device safety was characterized by tests showing safe deployment pressures and adequate sealing for emergency breaths. Safe deployment was evaluated by measuring the minimum pressure to evert elements of the tube in free space and navigate anatomy in an airway phantom. The sealing efficacy of each balloon configuration was measured in a simple tube model.

Free Eversion

The free eversion pressure of the tube configurations was determined by freely everting into a straight airway phantom, simulated by a plastic tube with an inner diameter of 3.7cm (Fig 4.6). Free eversion pressure is the pressure required to begin eversion, also known as *pressure above yield* [22]. This pressure is the minimum deployment pressure of the eversion device and was measured as the steady-state tube pressure during free eversion after overcoming spindle static friction (C, Fig. 4.8). Tube pressure was manually increased using the pressure regulator until steady-state eversion occurred.

Friction measurements were extracted from pressure transients (B, Fig. 4.8). The friction

effects of both spindle and balloon were measured as pressure peaks before free eversion began. Spindle friction is the static friction required to begin spindle rotation. Balloon everter friction is the kinetic friction between the balloon and the everter as the balloon element is drawn through the tube body. This can also be thought of as tail friction.

Balloon deployment pressures are the maximum tube pressures recorded just before the sudden volume increase associated with the deployment of a balloon.

Eversion Within Airway Phantom

The safety of an everted device in the airway was evaluated by recording the minimum deployment pressure of a plain tube (Config 0) past anatomies approximated in the phantom. The anatomical structures of interest include the lips, teeth and oral cavity, hard palate, soft palate, posterior pharyngeal wall, and esophageal sphincter, shown in Fig. 4.5. These anatomies are commonly damaged during intubation [9,26,33,44]. The posterior pharyngeal wall is of interest because manual intubation techniques exert enough pressure at this location to result in serious injury of the cervical spine in a patient with an unstable neck [26]. Insertion pressures were measured by placing an uninflated tube at the anatomy within the phantom and manually increasing tube pressure until it was able to evert past the anatomy under test.

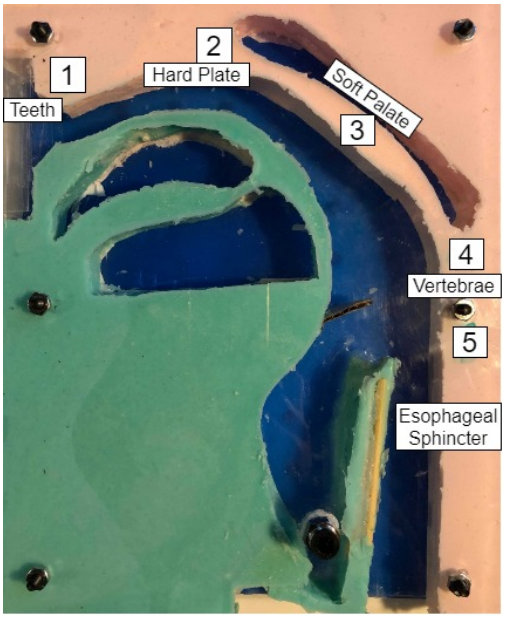

Figure 4.5: Scaled (2X) airway phantom with key anatomical areas highlighted. Hollow pockets in the silicon are included to simulate highly compliant areas of soft palate and tongue. A hinged flap simulates the epiglottis that covers the trachea during eating and drinking.

Balloon Sealing

The sealing performance of the balloon configurations is determined by two metrics: the maximum sealing pressure of the system and the maximum pressure supplied through the system. To evaluate these capabilities, the everted tube was pressurized to a specific Cuff Pressure (CP) (Fig. 4.6), and a back-pressure was supplied against the seal using a second pump operating at full rated voltage until steady-state pressure was achieved.

Air Delivery

The emergency breath supply capabilities of the tube were measured by similarly deploying and pressurizing a tube to a specific CP, then pumping air through the air delivery tube using

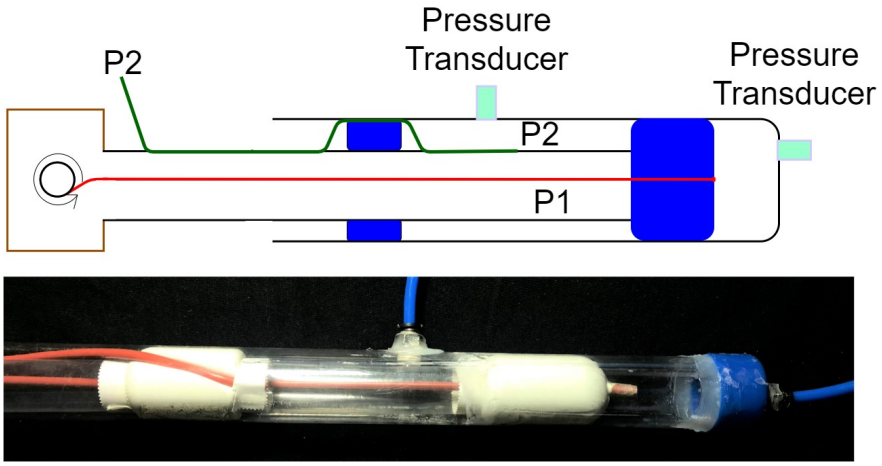

Figure 4.6: Clear rigid tube for evaluating free eversion pressures and sealing characteristics of tip and cuff balloons.

a 12V DC peristaltic pump or an adult-sized Bag-Valve-Mask (BVM) manual resuscitator (2000mL). The peristaltic pump gives the theoretical maximum supplied AWP, and the BVM provides peak and average AWP during pulmonary ventilation. All conditions and configurations in this and the two other experiments described were performed 5 times.

4.4 Results

4.4.1 Free Eversion

Free eversion pressure of a plain tube, Config 0, was 82 cmH_2O and increased by 14% with the side air delivery tube (Fig. 4.7). The eversion pressures of the tip and cuff balloons were 36% and 80% greater than the eversion pressure of Config 0, respectively. Balloon everter friction required the highest pressure to evert, 220 cmH_2O.

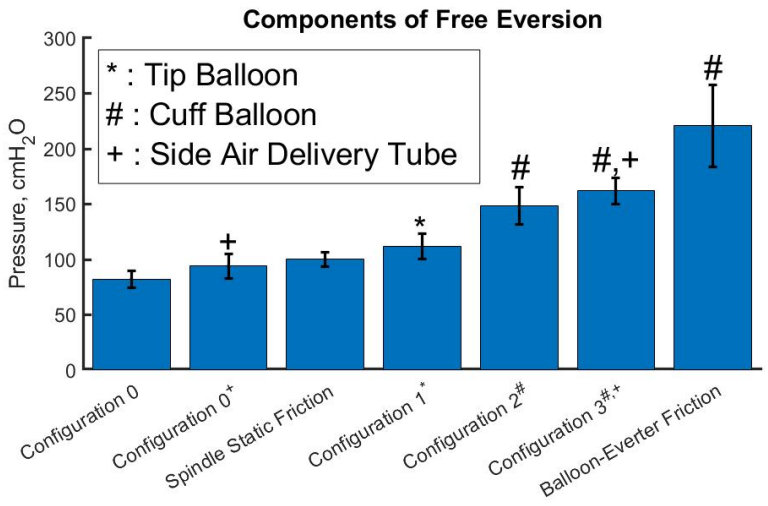

Figure 4.7: Eversion pressure thresholds of tube elements (Fig. 4.4) and static friction within the system. Error bars are standard deviation.

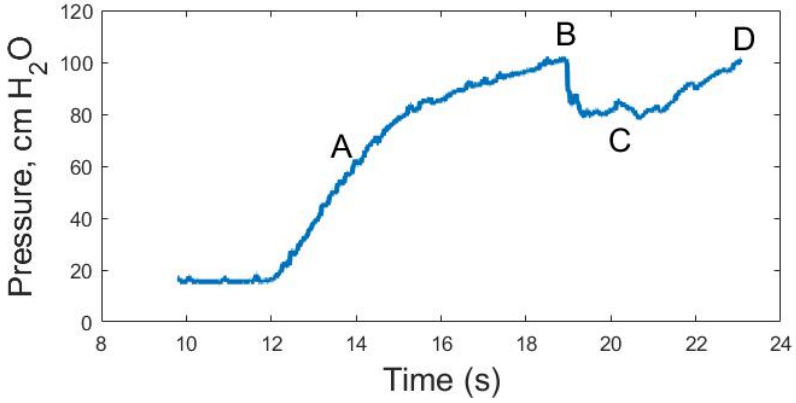

Figure 4.8: Representative time series pressure data of an everting tube. **A**- tube pressurizing (L = 0). **B**- static friction in spindle (L = 0), **C**- eversion begins, tube lengthens at constant pressure. **D**- tube is fully deployed and re-pressurizes to set point.

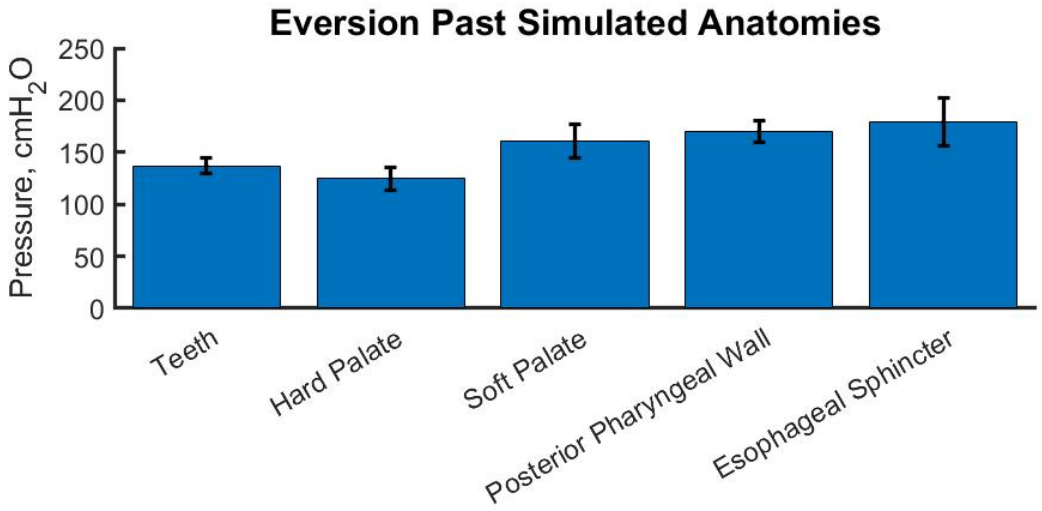

Figure 4.9: Eversion pressures required to evert a plain tube past key anatomy within the phantom. Error bars are standard deviation.

4.4.2 Eversion Within Airway Phantom

The peak eversion pressure within the phantom was 179 cmH_2O to evert past the esophageal sphincter and 137 cmH_2O to enter the phantom past the teeth (Fig. 4.9). Tube deployment pressures increased the farther the tube entered the simulated airway. Growth past the hard palate had the lowest eversion pressure of 124.7 cmH_2O and increased to 161 cmH_2O, 170 cmH_2O, and 179 cmH_2O to grow past the soft palate, posterior pharyngeal wall, and esophageal sphincter cmH_2O.

4.4.3 Balloon Sealing Efficacy

Configurations 1, 2 and 4 show 1:1 Cuff Pressure (CP) to sealing performance while configuration 3 is less effective at less than 1:2 (Fig. 4.10). Seal effectiveness less than 1:1 requires that CP must be higher than the airway pressure needed by the patient. Figure 4.10 also indicates that increasing CP corresponds to increasing levels of anatomical damage in the airway and performance characteristics of commercial devices.

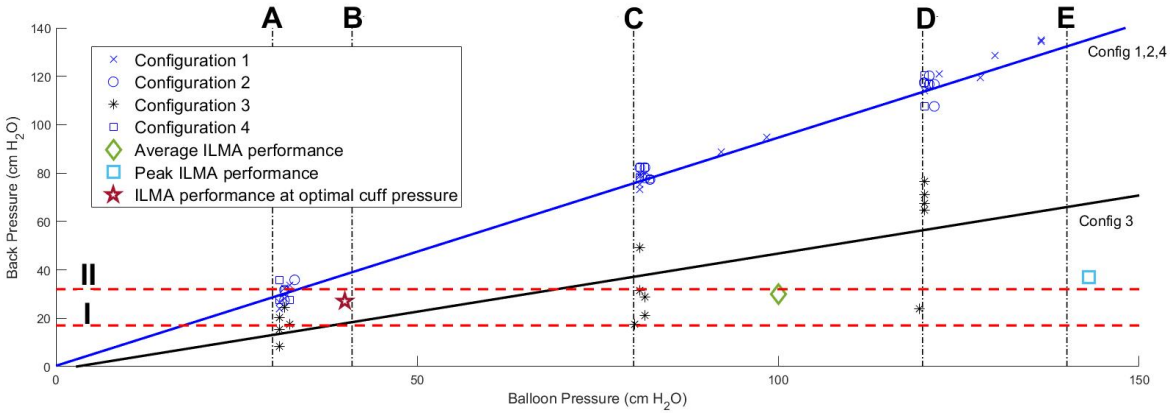

Figure 4.10: Sealing pressure of balloon configurations. Vertical bars indicate key mucosal pressure thresholds: **A**- optimal cuff pressure [7]; **B**- tracheal capillary perfusion pressures [26]; **C**- mucosal pressure at which pharyngeal capillaries collapse- [7]; **D**- advisable cuff pressure for LMA/ILMA-; and **E**- mucosal pressure at which pharyngeal mucosal perfusion stops, the patient is now at risk of ischemia. Horizontal lines represent performance of manual devices [36,49]. **I**- peak AWP supplied by Bag-Valve-Mask. **II**- peak Airway Pressure (AWP) supplied through a ventilator.

4.4.4 Air Delivery Though Balloon Configurations

Using a Bag-Valve-Mask (BVM), configuration 2 held the highest peak and average airway pressure of 42.13 and 12.1 cmH_2O, respectively (Table 4.2). Configuration 3 held the lowest peak and average airway pressure, 19.1 and 6.0 cmH_2O, respectively. Configurations 1 and 2 held the highest theoretical max AWP at 74.6 and 76 cmH_2O, and configuration 3 held the lowest theoretical max at 20.6 cmH_2O. The deployed configurations 1, 2, and 4 were able to supply higher peak AWP than manual devices in manikin studies [36, 46].

4.5 Discussion: Free Eversion

Free eversion pressure appeared to increase with increased material thickness and stiffness from added air tube and balloon elements. The cuff balloon's increased eversion pressure, compared to the tip balloon, is likely due to the tail friction. In the cuff construction, tail tension acts on the inextensible soft body, not the balloon itself, resulting in significant friction between the balloon and the cuff seam. In contrast, tail tension in the tip balloon acts on the highly elastic balloon, stretching it lengthwise as it deploys. This allows the tip balloon to bypass the seam without any tail friction. Although the cuff balloon has a higher deployment pressure, it is a more advantageous method of construction. It does not limit eversion after its deployment, whereas the tip balloon caps the everted tube eliminating the potential for any additional growth. Further growth after balloon deployment allows for a more flexible design and an increase in potential applications of these types of tubes.

Balloon everter friction required the highest tube pressure to overcome. For everted tube deployment into the airway, it is desirable to deploy the tube at the lowest and safest pressures to limit tissue damage. Sources of friction, such as balloon everter friction, should be considered and minimized during the design process.

4.6 Discussion: Eversion Within Phantom

Eversion pressures within the phantom indicate that an everted tube could safely deploy into the airway. Our everted tube shows maximum deployment pressures 36% and 20% less than the insertion pressures of the ILMA and LMAs, 28% on average. Maximum deployment pressure is 87% and 75% lower insertion pressures for Macintosh and Glidescope Laryngoscopes, 82% on average. The maximum force applied at the tip of the everted tube is approximately 8N at a CP of 179 cmH_2O, significantly less than forces applied during intubation, which are between 20N and 39N [26, 32]. In addition to insertion pressures, an ILMA exerts 394 cmH_2O during an up-down handle maneuver required to re-position a down-folded epiglottis. This maneuver would likely not be necessary for an everted airway: during deployment, the everted tube did not down-fold the epiglottis. However, the effects on deployment of the normally-closed esophageal sphincter still need to be investigated. An additional benefit is that everted tubes do not slide as they deploy, eliminating significant shear stress on airway tissues.

4.7 Discussion: Balloon Sealing Efficacy

Configurations 1, 2, and 4's sealing performance at the optimal CP of 30 cmH_2O is 32 cmH_2O on average this is comparable with the peak AWP supplied using a Medumat Transport Ventilator (31 cmH_2O) [49]. An AWP of 32 cmH_2O is also comparable to the performance of an ILMA at an average CP of 80 cmH_2O [26]. Configuration 3 could theoretically achieve AWP comparable with a ventilator at a CP of 70 cmH_2O and AWP comparable with BVM sealed AWP at a CP of 39 cmH_2O . Sealing at these pressures does limit perfusion but does not completely stop it. The optimal cuff pressure for a manual intubation device is 30 cmH_2O. At mucosal pressures greater than 34 cmH_2O , mucosal perfusion begins to decline as pharyngeal capillaries begin to collapse [7]. Manual devices are unable to seal adequate AWPs at this CP (Fig. 4.10) [7]. The recommended cuff pressure for manual intubation devices is 120 cmH_2O [7]. It is important to note that perfusion stops at 140 cmH_2O – when

the patient is at risk of ischemia [7].

The overall performance of everted balloons is promising. They are more compliant than LMA and ILMAs cuffs and can fully conform to the geometry of the airway without deforming or damaging the anatomy. In contrast, ILMA and LMA cuffs are composed of an inextensible balloon wrapped around a rigid preformed airway shape. Configuration 3 shows the lowest sealing performance. This is likely due to the side air delivery tube not sealing tightly against the phantom walls. Folds or wrinkles in the inflated balloon could allow for leaks in the seal.

4.8 Discussion: Airway Pressure Performance

Using an adult-sized BVM, all configurations sealed peak AWP greater than the literature value of 17 cmH_2O [36]. Configurations 1, 2, and 4 held theoretical AWP greater than all manual devices tested in a manikin including, an LMA, CombiTube, and Medumat Transport Ventilator; shown in table 4.2. These results indicate that an everted tube would be a viable solution for airway management at an emergency scene or a hospital. Sealing capabilities of configurations 1, 2, and 4 at low CP hold higher AWP than ILMAs, which require higher cuff pressures that nearly stop mucosal perfusion [26], [7].

Table 4.1: Forces Applied During Intubation

	Applied Pressure (cmH_2O)	**Applied Force** (N)
Everted Tube	179	8
ILMA [26]	273 - 394	-
LMA [26]	224	-
Macintosh Laryngoscope (Manikin) [8]	1,326	39
GlideScope Laryngoscope (Manikin) [8]	714	27
Macintosh Laryngoscope (in vivo) [32]	-	20

Table 4.2: Supplied Airway Pressures

	Average Pressure (cmH_2O)	**Peak Pressure (cmH_2O)**	**Theoretical Max (cmH_2O)**
BVM [36]	-	17	-
LMA [36]	-	21	-
CombiTube [36]	-	27	-
Medumat Transport Ventilator [49]	18.4	31	-
Compression Only [49]	1.3	3.9	-
Everted Config 1 *(Std Dev)*	8.6 (1.3)	25.5 (3.2)	74.6 (2)
Everted Config 2 *(Std Dev)*	12.1 (1.1)	42.1 (3.6)	76 (3.3)
Everted Config 3 *(Std Dev)*	6.0 (0.7)	19.1 (4.2)	20.6 (3)
Everted Config 4 *(Std Dev)*	9.7 (1.8)	32.8 (3.6)	54.6 (4.3)

Chapter 5

CONCLUSIONS AND FUTURE WORK

5.1 Inflated Beam Model

5.1.1 Limitations and Future Work

While the solution of an inflated cantilever beam is easy to compute and useful in static conditions, it does not have a closed-form solution. Determining theoretical max tip deflection or applied wall force from tip deflection requires iterative solving, which may be too slow for real-time control.

In the future, bi-axial testing of composite tube materials should be conducted to improve models of transverse buckling. Additionally, experiments should be done to extend these models to better describe the kinematics of everted tubes. Active pressure control should be studied for the kinematic control of everted tubes, thus maintaining the benefits of soft robots.

5.1.2 Conclusions

This study validates the current assumption that an everted tube can be modeled like an inflated beam. Our results confirm that the deflection and curvature of an LDPE everted tube can be accurately modeled using inflated beam theory. Beams composed of composite materials, like silicone-coated nylon, are not as accurately modeled. However, the model overestimates the exact buckling condition across all materials tested. Data indicates that everted tube buckling was better described by a maximum displacement rather than a maximum loading condition. The model can be iteratively solved to determine curvature from environmental displacements and applied loads to the environment.

5.2 Emergency Airway Device

5.2.1 Limitations and Future Work

Performance metrics were measured within a simplified straight phantom and a 2x silicone anatomy approximation but will soon be tested on an intubation manikin. To evaluate the emergency breath capabilities of an everted tube, a calibrated test lung and flow analyzer should be used to measure tidal volumes and flow rates from a ventilator. Interaction forces between the everted tube and airway tissues should be measured to provide a better indication of the device's safety.

5.2.2 Conclusions

The results of this study provide a starting place for additional research on the kinematics and modeling of everted tubes. Within a simplified phantom, deployment and air delivery performance show viability for advanced airway management. Furthermore, an everted tube's ability to passively navigate the airway ensures proper deployment. This eversion application can simplify the emergency airway management process for highly trained paramedics and bystanders alike.

BIBLIOGRAPHY

[1] Gary L. Atherton and John C. Johnson. Ability of paramedics to use the Combitube™ in prehospital cardiac arrest. *Annals of Emergency Medicine*, 22(8):1263–1268, 1993.

[2] Guanjun Bao, Lingfeng Chen, Yaqi Zhang, Shibo Cai, Fang Xu, Qinghua Yang, and Libin Zhang. Trunk-like Soft Actuator: Design, Modeling, and Experiments. *Robotica*, 38(May):732–746, 2019.

[3] Emelia J Benjamin, Paul Muntner, Alvaro Alonso, Marcio S Bittencourt, Clifton W Callaway, April P Carson, Alanna M Chamberlain, Alexander R Chang, Susan Cheng, Sandeep R Das, Francesca N Delling, Luc Djousse, Mitchell S V Elkind, Jane F Ferguson, Myriam Fornage, Lori Chaffin Jordan, Sadiya S Khan, Brett M Kissela, Kristen L Knutson, Tak W Kwan, Daniel T Lackland, Tené T Lewis, Judith H Lichtman, Chris T Longenecker, Matthew Shane Loop, Pamela L Lutsey, Seth S Martin, Kunihiro Matsushita, Andrew E Moran, Michael E Mussolino, Martin O'Flaherty, Ambarish Pandey, Amanda M Perak, Wayne D Rosamond, Gregory A Roth, Uchechukwu K A Sampson, Gary M Satou, Emily B Schroeder, Svati H Shah, Nicole L Spartano, Andrew Stokes, David L Tirschwell, Connie W Tsao, Mintu P Turakhia, Lisa B VanWagner, John T Wilkins, Sally S Wong, Salim S Virani, and On behalf of the American Heart Association Council on Epidemiology and Prevention Statistics Committee and Stroke Statistics Subcommittee. Heart disease and stroke statistics—2019 update: A report from the american heart association. *Circulation*, 139(10), 2019.

[4] P. Biro, P. Hofmann, D. Gage, Q. Boehler, C. Chautems, J. Braun, D. R. Spahn, and B. J. Nelson. Automated tracheal intubation in an airway manikin using a robotic endoscope: a proof of concept study. *Anaesthesia*, page anae.14945, jan 2020.

[5] Megan B. Blackburn, Michael D. April, Derek J. Brown, Robert A. DeLorenzo, Kathy L. Ryan, August N. Blackburn, and Steven G. Schauer. Prehospital airway procedures performed in trauma patients by ground forces in Afghanistan. *The journal of trauma and acute care surgery*, 85(1S Suppl 2):S154–S160, 2018.

[6] Laura H. Blumenschein, Margaret M. Coad, David A. Haggerty, Allison M. Okamura, and Elliot W. Hawkes. Design, Modeling, Control, and Application of Everting Vine Robots. *Frontiers in Robotics and AI*, 7(November):1–24, 2020.

[7] Joseph Brimacombe, Christian Keller, and Fritz Pühringer. Pharyngeal Mucosal Pressure and Perfusion . *Anesthesiology*, 91(6):1661–1661, 1999.

[8] M. Carassiti, R. Zanzonico, S. Cecchini, S. Silvestri, R. Cataldo, and F. E. Agrò. Force and pressure distribution using Macintosh and GlideScope laryngoscopes in normal and difficult airways: A manikin study. *British Journal of Anaesthesia*, 108(1):146–151, 2012.

[9] M. Chandler. Tracheal intubation and sore throat: A mechanical explanation. *Anaesthesia*, 57(2):155–161, 2002.

[10] Margaret M. Coad, Laura H. Blumenschein, Sadie Cutler, Javier A. Reyna Zepeda, Nicholas D. Naclerio, Haitham El-Hussieny, Usman Mehmood, Jee-hwan Ryu, Elliot W. Hawkes, and Allison M. Okamura. Vine Robots: Design, Teleoperation and Deployment for Navigation and Exploration. *IEEE Robotics and Automation Magazine*, 21(1):1–9, 2020.

[11] Margaret M Coad, Rachel P Thomasson, Laura H Blumenschein, Nathan S Usevitch, Elliot W Hawkes, and Allison M Okamura. Retraction of Soft Growing Robots without Buckling. *IEEE Robotics and Automation Letters*, 5(2):2115–2122, 2020.

[12] R. L. Comer and Samuel Levy. Deflections of an inflated circular-cylindrical cantilever beam. *AIAA Journal*, 1(7):1652–1655, 1963.

[13] Brian H. Do, Valory Banashek, and Allison M. Okamura. Dynamically Reconfigurable Discrete Distributed Stiffness for Inflated Beam Robots. *Proceedings - IEEE International Conference on Robotics and Automation*, pages 9050–9056, 2020.

[14] Volker Dörges, Volker Wenzel, Eicke Neubert, and Peter Schmucker. Emergency airway management by intensive care unit nurses with the intubating laryngeal mask airway and the laryngeal tube. *Critical Care*, 4(6):369–376, 2000.

[15] Brian J. Eastridge, Robert L. Mabry, Peter Seguin, Joyce Cantrell, Terrill Tops, Paul Uribe, Olga Mallett, Tamara Zubko, Lynne Oetjen-Gerdes, Todd E. Rasmussen, Frank K. Butler, Russell S. Kotwal, John B. Holcomb, Charles Wade, Howard Champion, Mimi Lawnick, Leon Moores, and Lorne H. Blackbourne. Death on the battlefield (2001-2011): Implications for the future of combat casualty care. *Journal of Trauma and Acute Care Surgery*, 73(6 SUPPL. 5), 2012.

[16] Ioannis Exarchos, Brian H. Do, Fabio Stroppa, Margaret M. Coad, Allison M. Okamura, and C. Karen Liu. Task-Specific Design Optimization and Fabrication for Inflated-Beam Soft Robots with Growable Discrete Joints. 2021.

[17] W. B. Fichter. A theory for inflated thin-wall cylindrical beams. *Computer and Structures*, 3(1):203–209, 1966.

[18] B. Raymond Fink, Roy W. Martin, and Charles A. Rohrmann. Biomechanics of the human epiglottis. *Acta Oto-Laryngologica*, 87(3-6):554–559, 1979.

[19] Joseph D. Greer, Laura H. Blumenschein, Allison M. Okamura, and Elliot W. Hawkes. Obstacle-Aided Navigation of a Soft Growing Robot. *Proceedings - IEEE International Conference on Robotics and Automation*, 2:4165–4172, 2018.

[20] Joseph D. Greer, Tania K. Morimoto, Allison M. Okamura, and Elliot W. Hawkes. Series pneumatic artificial muscles (sPAMs) and application to a soft continuum robot. *Proceedings - IEEE International Conference on Robotics and Automation*, pages 5503–5510, 2017.

[21] David A. Haggerty, Nicholas D. Naclerio, and Elliot W. Hawkes. Characterizing Environmental Interactions for Soft Growing Robots. *IEEE International Conference on Intelligent Robots and Systems*, pages 3335–3342, 2019.

[22] Elliot W. Hawkes, Laura H. Blumenschein, Joseph D. Greer, and Allison M. Okamura. A soft robot that navigates its environment through growth, 2017.

[23] T. M. Hemmerling, R. Taddei, M. Wehbe, C. Zaouter, S. Cyr, and J. Morse. First robotic tracheal intubations in humans using the Kepler intubation system. *British Journal of Anaesthesia*, 2012.

[24] Whei Jung and Joonghee Kim. Factors associated with first-pass success of emergency endotracheal intubation. *American Journal of Emergency Medicine*, 38(1):109–113, 2020.

[25] Mitsuhiro Kano, Yoshinaka Shimizu, Keisuke Okayama, Toshirou Igari, and Masayoshi Kikuchi. A morphometric study of age-related changes in adult human epiglottis using quantitative digital analysis of cartilage calcification. *Cells Tissues Organs*, 180(2):126–137, 2005.

[26] Christian Keller and Joseph Brimacombe. Pharyngeal Mucosal Pressures, Airway Sealing Pressures, and Fiberoptic Position with the Intubating versus the Standard Laryngeal Mask Airway. *Anesthesiology*, 90(4):1001–1006, apr 1999.

[27] Richard A Lazar. The aed shortage.

[28] Dong Keon Lee, Dong Hyuck Shin, Seung M.I.N. Park, Yong Hwan Kim, Sang O Park, and Young Hwan Lee. I-gel as a first-line airway device in the emergency room for patients with out-of-hospital cardiac arrest. *Signa Vitae*, 14(2):61–65, 2018.

[29] Daniel P. Lefrançois and Daniel G. Dufour. Use of the esophageal tracheal combitube™ by basic emergency medical technicians. *Resuscitation*, 52(1):77–83, 2002.

[30] Robert W. Leonard, George W. Brooks, and Harvey G. McComb Jr. Structural considerations of inflatable reentry vehicles. (September), 1960.

[31] Jamie Luong, Paul Glick, Aaron Ong, Maya S. DeVries, Stuart Sandin, Elliot W. Hawkes, and Michael T. Tolley. Eversion and retraction of a soft robot towards the exploration of coral reefs. *RoboSoft 2019 - 2019 IEEE International Conference on Soft Robotics*, (April):801–807, 2019.

[32] E. P. McCoy, B. A. Austin, R. K. Mirakhur, and K. C. Wong. A new device for measuring and recording the forces applied during laryngoscopy. *Anaesthesia*, 50(2):139–143, 1995.

[33] Pavel Michalek, William Donaldson, Eliska Vobrubova, and Marek Hakl. Complications associated with the use of supraglottic airway devices in perioperative medicine, 2015.

[34] Daisuke Mishima, Takeshi Aoki, and Shigeo Hirose. Development of pneumatically controlled expandable arm for search in the environment with tight access. In *Field and Service Robotics*, Springer Tracts in Advanced Robotics, pages 509–518. Springer Berlin Heidelberg, Berlin, Heidelberg, 2006.

[35] Christopher Newell, Scott Grier, and Jasmeet Soar. Airway and ventilation management during cardiopulmonary resuscitation and after successful resuscitation, 2018.

[36] Hartmut Ocker, Volker Wenzel, Peter Schmucker, and Volker Dörges. Effectiveness of various airway management techniques in a bench model simulating a cardiac arrest patient. *Journal of Emergency Medicine*, 20(1):7–12, 2001.

[37] Panagiotis Polygerinos, Nikolaus Correll, Stephen A. Morin, Bobak Mosadegh, Cagdas D. Onal, Kirstin Petersen, Matteo Cianchetti, Michael T. Tolley, and Robert F. Shepherd. Soft Robotics: Review of Fluid-Driven Intrinsically Soft Devices; Manufacturing, Sensing, Control, and Applications in Human-Robot Interaction, dec 2017.

[38] Mark Runciman, Ara Darzi, and George P. Mylonas. Soft Robotics in Minimally Invasive Surgery. *Soft Robotics*, 6(4):423–443, aug 2019.

[39] Daniela Rus and Michael T. Tolley. Design, fabrication and control of soft robots. *Nature*, 521(7553):467–475, 2015.

[40] Ankit Saxena, Eric M. Paul, Randy S. Haluc, Barry Fell, and Jason Moore. Tubular locomotion and positioning using tip eversion for endoscopy. *Journal of Medical Devices, Transactions of the ASME*, 14(2):1–5, 2020.

[41] M. Selvaggio, L. A. Ramirez, N. D. Naclerio, B. Siciliano, and E. W. Hawkes. An obstacle-interaction planning method for navigation of actuated vine robots. *Proceedings - IEEE International Conference on Robotics and Automation*, pages 3227–3233, 2020.

[42] Patrick Slade, Alex Gruebele, Zachary Hammond, Michael Raitor, Allison M. Okamura, and Elliot W. Hawkes. Design of a soft catheter for low-force and constrained surgery. *IEEE International Conference on Intelligent Robots and Systems*, 2017-Septe:174–180, 2017.

[43] Thomas George Thuruthel, Egidio Falotico, Federico Renda, and Cecilia Laschi. Learning dynamic models for open loop predictive control of soft robotic manipulators. *Bioinspiration & Biomimetics*, 12(6):066003, oct 2017.

[44] Abdelfattah A. Touman and Grigoris K. Stratakos. Long-Term Complications of Tracheal Intubation. *Tracheal Intubation*, 2018.

[45] SL L Veldman. *Design and analysis methodologies for inflated beams*. 2005.

[46] Henry E. Wang, Judith R. Lave, Carl A. Sirio, and Donald M. Yealy. Paramedic intubation errors: Isolated events or symptoms of larger problems? *Health Affairs*, 25(2):501–509, 2006.

[47] Xinyu Wang, Yuanfa Tao, Xiandong Tao, Jianglong Chen, Yifeng Jin, Zhengxiang Shan, Jiyang Tan, Qixin Cao, and Tiewen Pan. An original design of remote robot-assisted intubation system. *Scientific Reports*, 8(1), 2018.

[48] Michael Wehner, Michael T. Tolley, Yiğit Mengüç, Yong Lae Park, Annan Mozeika, Ye Ding, Cagdas Onal, Robert F. Shepherd, George M. Whitesides, and Robert J. Wood. Pneumatic Energy Sources for Autonomous and Wearable Soft Robotics. *Soft Robotics*, 1(4):263–274, 2014.

[49] Bernd E. Winkler, Ralf M. Muellenbach, Thomas Wurmb, Manuel F. Struck, Norbert Roewer, and Peter Kranke. Passive continuous positive airway pressure ventilation during cardiopulmonary resuscitation: a randomized cross-over manikin simulation study. *Journal of Clinical Monitoring and Computing*, 31(1):93–101, 2017.